Langmuir

Article

pubs.acs.org/Langmuir

Nanometric Resolution in the Hydrodynamic Size Analysis of Ligand-Stabilized Gold Nanorods

Jonathan G. Mehtala and Alexander Wei*

Department of Chemistry, Purdue University, 560 Oval Drive, West Lafayette, Indiana 47907, United States

Supporting Information

ABSTRACT: The stability and hydrodynamic size of ligand-coated gold nanorods (GNRs; aspect ratio 3.6) have been characterized by nanoparticle tracking analysis (NTA)—a single-particle counting method that can measure size distributions with low nanometer resolution. Stable aqueous suspensions of citrate-stabilized GNRs (cit-GNRs) are amenable to surface functionalization without loss of dispersion control. Cit-GNRs can be treated with chemisorptive ligands (thiols and dithiocarbamates), nonionic surfactants (Tween 20), and proteins (human serum albumin), all of which produce stable suspensions at low surfactant concentrations. The precision of NTA (relative standard deviation 10−12%, standard error <2%) is sufficient to allow differences in the hydrodynamic size of coated GNRs to be interpreted in terms of surfactant structure and conformation.

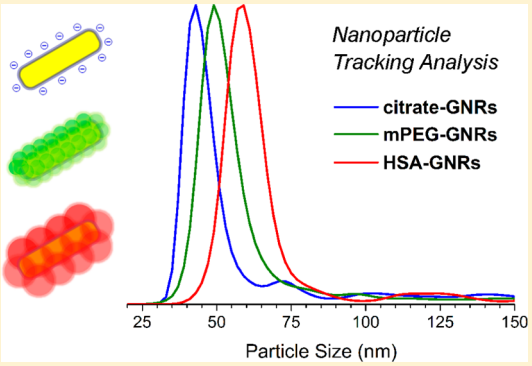

INTRODUCTION

Particle size analysis is fundamental to nanomaterials characterization but must be conducted in an appropriate context. Nanoparticle analysis by transmission electron microscopy (TEM) is arguably one of the more popular methods but is typically performed in a dry or vacuum state and is challenged by low particle counts. TEM is also less appropriate for estimating the hydrodynamic (HD) size of nanoparticles in solution, especially those with organic layers of unknown thickness. Statistically robust methods for HD analysis include dynamic light scattering (DLS), tunable resistive pulse sensing (TRPS), and nanoparticle tracking analysis (NTA).[1,2] DLS uses a second-order correlation function to convert fluctuations in scattering intensity into a one-dimensional parameter defining hydrodynamic size (d_h).[3] While DLS supports high sampling volumes ($N = 10^4-10^5$), its peak distributions are broad (effective resolution >30%) and requires an intensity-weighted correction factor (*Z*-average) due to size-dependent scattering.[4] TRPS is an electrokinetic method that measures the d_h of nanoparticles passing through nanopores of defined size.[5] TRPS offers better resolution than DLS but is only useful for particles above 60 nm, limited by the pore diameter of the supporting membrane.

NTA produces size distributions by recording the Brownian motion of thousands of individual particles under optical darkfield conditions.[2,6] From the Stokes−Einstein equation, d_h can be expressed simply as

$$d_h = \frac{4k_B T \Delta t}{3\pi\eta\langle(x, y)^2\rangle} \quad (1)$$

where k_B is the Boltzmann constant, T is temperature, Δt is recording time per frame (~0.02 s), η is viscosity, and $\langle(x,y)^2\rangle$ is mean-squared displacement in two dimensions.[6] NTA is capable of tracking nanoparticles at moderate volumes (sample size $N = 10^3-10^4$) and can record d_h values as small as 20 nm, depending on the particles' scattering cross sections.[7] In addition, recent developments in NTA data processing can be applied to produce d_h values with relative standard deviations (RSDs) of 10−12%.[8]

NTA has become an accepted method for characterizing colloidal size distributions in aqueous suspensions[1] and can also measure incremental changes in HD size as a function of surface conjugation. For example, James and Driskell have reported size changes in colloidal gold nanoparticles exposed to protein A at various concentrations, reminiscent of an adsorption isotherm.[9] However, NTA has not been fully validated for anisotropic particles such as gold nanorods (GNRs)[10] due to possible complications in data analysis introduced by additional diffusion tensors[11,12] as well as challenges in preparing anisotropic particles of sufficient uniformity and purity.

The presence of residual surfactants is a also potentially confounding factor in the HD analysis of colloidal suspensions, as it can compromise dispersion quality by promoting interparticle attraction instead of repulsion.[13−15] As a case in point, GNRs with low aspect ratio (AR < 4) can be synthesized with narrow size dispersity (10−15%) in the presence of cetyltrimethylammonium bromide (CTAB), a micellar surfactant.[16,17] However, the HD analysis of diluted GNR suspensions can produce variable outcomes: samples with

Received: July 25, 2014
Revised: October 23, 2014
Published: October 28, 2014

   dx.doi.org/10.1021/la502955h | *Langmuir* 2014, 30, 13737−13743

excess CTAB (>1 mM) are contaminated with micelles, whereas NTA of GNRs with low levels of CTAB (<10 μM) produce multiple or asymmetric mode peaks,[10] suggestive of incomplete dispersion. The removal of residual CTAB from GNRs is a vexing problem; in addition to particle aggregation,[15] its persistence can contribute toward cytotoxicity[18] and nonspecific cell uptake.[19] This issue has recently been resolved by a protocol that reliably exchanges CTAB with citrate, using polystyrenesulfonate (PSS) as a detergent to remove residual surfactant.[20]

Here we show that NTA can precisely characterize the hydrodynamic size of low-aspect-ratio GNRs stabilized with citrate (cit-GNRs). The d_h values obtained from NTA correlate closely with GNR length, with greater accuracy and precision than DLS[1,4] and with comparable resolution to TEM. The cit-GNRs are also readily functionalized with other ligands using standard surface exchange methods[21] and can be evaluated by NTA to reveal incremental changes in d_h as a function of ligand or surfactant structure.

EXPERIMENTAL SECTION

All materials were obtained from Sigma-Aldrich unless otherwise noted. Poly(ethylene glycol) (PEG) derivatives were obtained from Nanocs, Inc. Recombinant human serum albumin (HSA) was kindly provided by Prof. Greg Knipp (College of Pharmacy, Purdue University). Deionized water was obtained from an ultrafiltration system (Milli-Q, Millipore) with a measured resistivity above 18 MΩ·cm and passed through a 0.22 μm filter. Particle-free water for NTA analysis was obtained in polyethylene containers from a local supermarket.

Preparation of Citrate-Stabilized GNRs. GNRs were synthesized on a 200 mL scale in 0.1 M CTAB solutions at an optical density (OD) of 1.3 using previously reported methods.[16,17] Excess CTAB was removed by subjecting GNRs to centrifugation and redispersion (C/R) in water, followed by three rounds of C/R using dilute solutions of Na-PSS (M_w = 70 kDa) as described in a companion paper.[20] The PSS-washed GNRs were then subjected to two C/R cycles using 5 mM sodium citrate (Na_3-cit), yielding stable suspensions of citrate-coated GNRs (cit-GNRs) with OD values ranging from 6 to 12.

Surface Functionalization of Cit-GNRs. In a typical experiment, 0.1 mL of cit-GNRs (OD 7.5) was diluted with 3 mL of water, centrifuged for 30 min at 7500*g*, and then carefully separated from the supernatant. A 0.9 mL solution of 5 kDa mPEG-thiol (0.7 wt % in water) was prepared separately and treated with 0.1 mL of 15 mM $NaBH_4$ for 30 min to reduce residual disulfides and then combined with the pelleted GNRs by vortex mixing. After 12 h, the redispersed GNRs were centrifuged at 7500*g* for 30 min, and redispersed in water to a final volume of 1 mL. Similar procedures were performed using other surfactant solutions (PEG-dithiocarbamate,[19] Tween-20, HSA) without $NaBH_4$ treatment. Mercaptoundecanoic acid (MUA)-stabilized GNRs were prepared by treating 0.75 mL of cit-GNRs in water (OD 0.6) with 0.25 mL of 4 mM MUA in EtOH for 20 h, then diluted with 2 mL of water, centrifuged at 7500*g* for 30 min, and then redispersed in 1 mL of water.

Particle Characterization. Absorbance spectra were recorded using a Cary Bio50 spectrophotometer (Varian). TEM images were obtained using a Philips CM-10 (FEI) with an accelerating voltage of 100 kV. DLS and zeta potential analysis was performed with a ZetaSizer Nano (Malvern Instruments; λ = 633 nm); data analysis was supported by Zetasizer v.7.02. DLS was performed in glass cuvettes or disposable capillary cells (DTS 1060C), with an assumed viscosity for water at 25 °C (η = 0.8872 mPa) and refractive indices for water and Au at 633 nm (n = 1.330 and 0.2). Samples were allowed to equilibrate for 30 s inside the instrument prior to analysis; measurements were then accumulated over 12−16 runs at rates of 30−70 kcps.

NTA was performed using a Nanosight LM-10 system (Malvern Instruments) with 405 nm laser excitation and particle-free distilled water stored in polyethylene containers. Data analysis was supported by NTA v.2.3.5.0033 (Build 16). The imaging chamber was cleaned with acetone and a microfiber cloth prior to use and then rinsed until no background signals were observed. Water was removed from the NTA chamber with a sterile plastic syringe just prior to use and replaced with a dilute solution of surfactant-stabilized GNRs (100 μL, OD 0.01−0.05). Coated GNRs were prepared using the surfactant concentrations described above (initial OD 0.4−2.0) and then diluted 20−150-fold just prior to NTA. Five tracking videos were collected per sample; 50 μL of fresh solution was injected in between each run to prevent particles from settling, followed by a 60 s recording at a shutter speed of 700 and a gain of 400. A minimum of 2000 particle tracks were recorded, which yielded d_h values based on mode peak analysis. Optimized parameters for video analysis (advanced mode) included a detection threshold of 18, a 9 × 9 blur setting, and automated settings for track length and minimum particle size. Statistical analysis of GNR size distribution was performed by applying Gaussian fits to the mode peaks. Finally, calibration measurements on standardized 100 nm polystyrene beads were routinely performed to ensure the accuracy of the NTA studies.

RESULTS AND DISCUSSION

Characterization and Size Analysis of Citrate-Stabilized GNRs. TEM analysis of the cit-GNRs indicated a mean length and width of 44.4 ± 3.9 nm and 12.2 ± 1.2 nm, respectively, corresponding to a RSD of 8.8% (Figure 1a). The uniform quality of the cit-GNRs was supported by absorbance spectroscopy (Figure 1b and Figure S1, Supporting Information), which produced a peak centered at 815 nm with a full width at half-maximum (fwhm) of 138 nm (0.26 eV). HD size distribution by NTA produced values remarkably close to the GNR lengths determined by TEM. Mode peaks accumulated over five separate runs (N_{track} = 2400−3200 each) yielded an average d_h of 43.4 nm (standard error = 0.75 nm); a Gaussian fit of the mode peak produced a d_h of 43.8 nm with a standard deviation of 5.0 nm (RSD 11.4%), well within the error of TEM measurement (Figure 1c).

The NTA mode peaks are much narrower than those produced by DLS using intensity-weighted size distributions (the standard practice for HD analysis). In a direct comparison, z-weighted DLS signals accumulated over 1 min (N = 2.6 × 10^5) at 260 kcps yielded a mode d_h value of 51 nm; the RSD of the corresponding Gaussian fit was more than 30%. We note that (i) Gaussian fits of DLS mode peaks ignore skewness and kurtosis within the data, but allow us to compare the precision of each technique to the first approximation, and (ii) the comparison between NTA and DLS is not absolute, as the size distribution for the latter is based on scattering intensity rather particle count. Nevertheless, the large differences in peak resolution are more than sufficient to illustrate the advantages of NTA over DLS for HD size analysis.

NTA is also a sensitive gauge of dispersion quality, much more so than absorbance spectroscopy, a convenient but crude method that relies on changes in the surface plasmon band.[22,23] For example, cit-GNRs in 5 mM Na_3-cit (pH 7.3) produced a d_h peak approaching normal distribution, corresponding with <1% aggregation by peak area integration (Figure 2a), while the NTA plot of PSS-GNRs in 0.4 wt % Na-PSS (pH 5) revealed a multimodal distribution, indicating partial aggregation (Figure 2b). In contrast, the absorbance spectra for cit-GNRs and PSS-GNRs are nearly identical; while the latter has lower transmission below 650 nm and a slightly larger fwhm at plasmon resonance (Figure 1b), it hardly suggests the presence of aggregates. We note that while the end-to-end assembly of GNRs can produce large shifts in longitudinal plasmon

dx.doi.org/10.1021/la502955h | Langmuir 2014, 30, 13737−13743

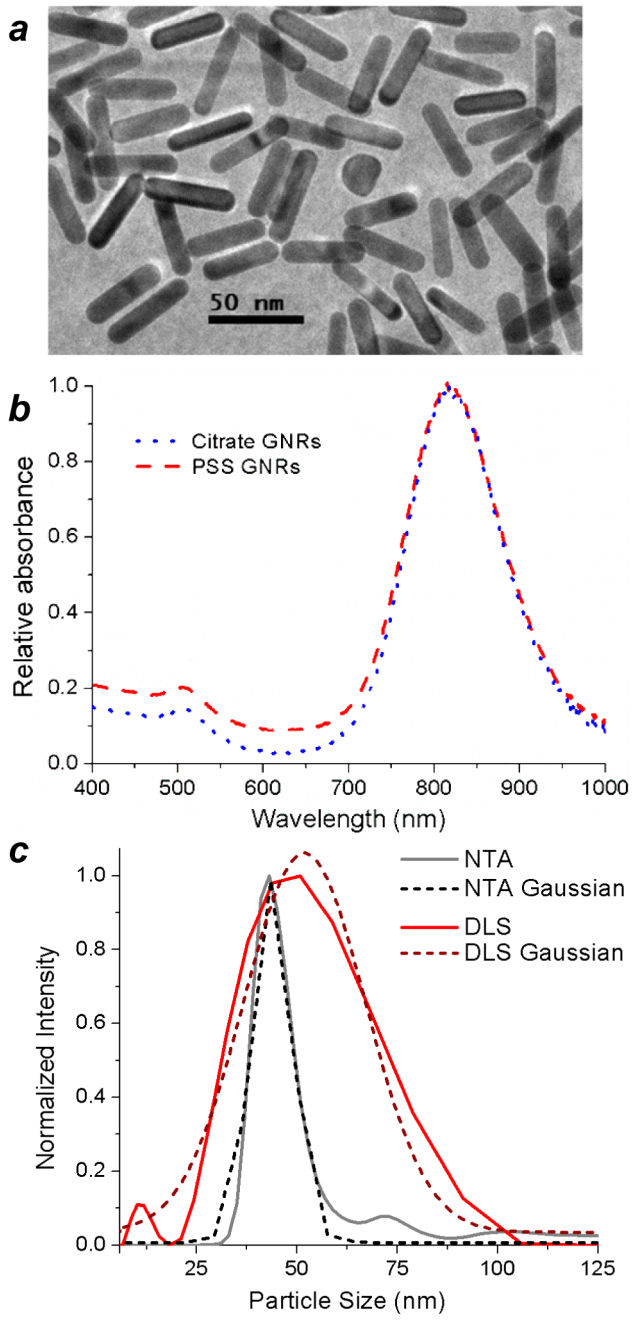

Figure 1. (a) TEM image of cit-GNRs (44.4 × 12.2 nm; 8.8% RSD). (b) Absorption spectrum of diluted cit-GNR dispersion (λ_{LPR} = 815 nm), prepared from PSS-GNRs.[20] (c) HD size analysis of cit-GNRs using NTA (black; 43.4 nm; 11.4% RSD) versus DLS (red; 51 nm; 31% RSD). RSDs are derived from Gaussian fits (dashed). The NTA size distribution is number-based (N_{track} = 1.44 × 10^4), whereas the DLS size distribution is intensity-based (N = 2.60 × 10^5).

resonance,[24−27] the aggregation of GNRs in other orientations does not lead to pronounced changes. Earlier works have shown that side-by-side aggregation can produce modest blue-shifts in transverse plasmon resonance ($\lambda \sim 520$ nm), but the extent of such shifts depends strongly on interparticle distances.[23,28] Overall, NTA provides the strongest evidence that cit-GNRs are fully dispersed and experience minimum aggregation in the absence of other surfactants.

It is worthwhile to present a balanced discussion on the use of NTA for characterizing the HD size of anisotropic particles, which are known to exhibit different motional behavior than spheres.[11,12,29] Strictly speaking, particle sizes derived from the Stokes−Einstein equation are based on a spherical model with a single diffusion coefficient, which equates the d_h of anisotropic particles to that of a sphere with the same translational mobility. In fact, the Brownian motion of axially symmetric particles can be described using separate diffusion coefficients for coaxial and transverse translation ($D_\parallel$ and $D_\perp$) as well as rotation (D_θ). Translational and rotational diffusion are coupled in the fast (autocorrelation) regime but are essentially independent for displacements measured over longer periods. The autocorrelation time of low-aspect GNRs in water has been estimated to be on the order of 50 μs,[30] which is several orders of magnitude shorter than the MSD time steps recorded by NTA, meaning that HD analysis is unaffected by D_θ.

With respect to the anisotropy of translational diffusion, the ratio of $D_\parallel$ to $D_\perp$ depends partly on aspect ratio but is also affected by boundary conditions imposed on particle motion. Single-particle tracking studies of submicron ellipsoids have shown that diffusion anisotropy increases for particles confined to two dimensions (attributable to friction anisotropy),[11,12] but rodlike particles with unrestricted mobility in three dimensions exhibit low anisotropy ($D_\parallel/D_\perp < 2$), even with high aspect ratios.[31,32] While NTA measurements are quasi-two-dimensional (bounded by the thickness of the focal plane),[6] particles can freely move in all directions which favors isotropic diffusion. Further evidence for isotropic Brownian motion can also be obtained by analyzing the tracking videos for vectored flow and used to determine an acceptable threshold in aspect ratio. NTA can thus be applied toward the HD analysis of anisotropic nanoparticles with these considerations in mind, and the d_h values can be collated with an independent sizing method such as TEM analysis for a more precise interpretation.

Surface Modification of Citrate-Stabilized GNRs. Citrate-stabilized colloids have been used for decades in the preparation of imaging contrast agents.[33,34] It is therefore not surprising that surface functionalization with cit-GNRs is facile, with fewer problems in dispersion quality than CTAB- or PSS-stabilized GNRs (for more details see Figure S2, Supporting Information). We note that other stabilizing agents such as phosphatidylcholine,[35] animomercaptotriazole,[36] and mercaptocarboxylic acids[37] have also been examined as biocompatible surrogates in place of CTAB; nevertheless, citrate-stabilized colloids are among the most highly trusted substrates for preparing surface-modified nanoparticles.

The effects of ligand adsorption on cit-GNRs after a single round of treatment were again characterized by NTA and absorbance spectroscopy (Figure 3 and Figure S3; Table 1). Small thiols such as mercaptoundecanoic acid (MUA; MW 218) could stabilize GNR dispersions without a significant change in the mode d_h value, while larger ligands such as mPEG thiol or dithiocarbamate (M_w = 1 or 5 kDa) increased d_h by 5−7 nm. This supports the assumption that chemisorptive ligands adsorb as monolayers on GNR surfaces; however, HD size does not increase monotonically with molecular weight. The experimental data suggests that the 1 kDa PEG chains may adopt partially extended conformations, whereas the 5 kDa mPEG chains are presumed to adopt mushroom-like conformations, in accord with previous studies.[38] We note that GNRs coated with 1 kDa PEG thiol also produce a relatively broad NTA peak, suggesting incomplete dispersion control.

dx.doi.org/10.1021/la502955h | Langmuir 2014, 30, 13737−13743

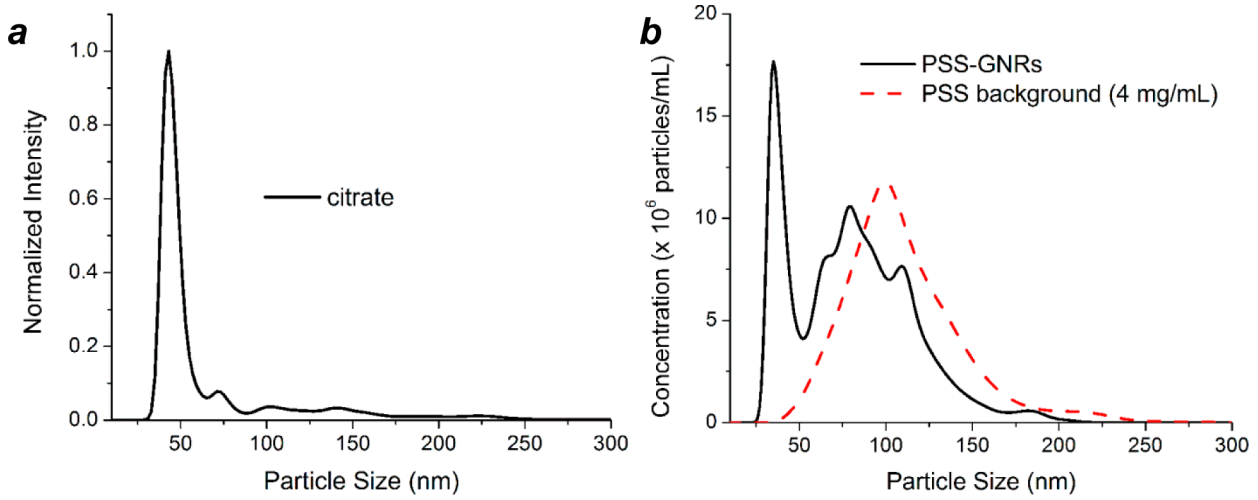

Figure 2. Nanoparticle tracking analysis of (a) cit-GNRs in 5 mM Na_3-cit (pH 7.3) and (b) PSS-GNRs in 0.4 wt % Na-PSS (pH 5), at similar particle concentrations (ca. 2×10^9 GNRs/mL). The latter shows a large number of aggregates in the 75−200 nm range, assumed to be a composite of polymer and GNRs (PSS background provided for comparison).

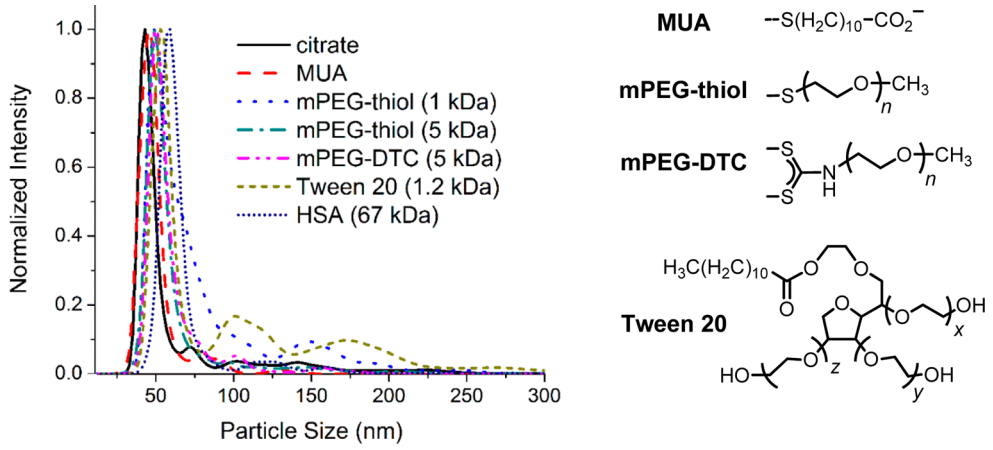

Figure 3. NTA of surfactant-modified GNRs, prepared from cit-GNRs. Coated GNR samples (initial OD 0.60−0.75) were diluted 20−30-fold (final OD 0.02−0.05) prior to NTA. Intensities are normalized to enable a comparison between mode peaks as a function of ligand coating.

Table 1. Hydrodynamic Size and Charge of Surface-Modified GNRs after Ligand Adsorption[a]

GNR coating	surfactant conc	d_h[b] (nm)	ζ-potential[c] (mV)
citrate	5 mM	44 ± 8	−27 ± 13[d]
MUA	1 mM	45 ± 6	−37 ± 14
mPEG-thiol (1 kDa)	1.5 mM (0.15 wt %)	49 ± 11	−9 ± 7
mPEG-thiol (5 kDa)	1.5 mM (0.75 wt %)	49 ± 6	−7 ± 9
mPEG-DTC (5 kDa)	1 mM (0.5 wt %)	51 ± 6	−14 ± 6
Tween 20 (1.2 kDa)	5 mM	53 ± 6	−19 ± 8
HSA (66 kDa)	1 wt %	59 ± 6	−11 ± 8

[a]See Experimental Section for details. [b]Obtained by NTA; SD from Gaussian fit of mode peak (accumulated over 5 runs). [c]Measured in diluted PBS (I =1 mM; pH 7.4). [d]Measured in diluted PBS ($I \sim 8.2$ mM) adjusted to pH 9.5.

Treatment of cit-GNRs with Tween 20 (1.2 kDa; 5 mM) increased the mode d_h by 9 nm, greater than that produced by chemisorptive mPEG species. Tween 20 has been reported to form micelles of 7−9 nm,[39] comparable to the observed increase in HD size. NTA also revealed minor populations of submicron particles (broad peaks centered at 100 and 175 nm) that can be attributed to aggregates containing two or more GNRs. This shows that while nonionic surfactants may be useful as nanoparticle dispersants, they do not provide full control over surface properties; indeed, the ζ-potential of GNRs treated with Tween 20 remains moderately negative (Table 1), indicating coadsorption of residual citrate. Lastly, exposing cit-GNRs to human serum albumin (HSA, 67 kDa; 1 wt %) increased d_h by 15 nm, which is consistent with a monolayer of HSA in its native conformation,[40,41] but thicker than that adsorbed on hydrophobic nanoparticles.[42] We note that DLS is often used to estimate the thickness of biomacromolecular coatings on nanoparticles,[41,43,44] but its precision is not as high as NTA as demonstrated earlier (cf. Figure 1c).[1,2]

To determine whether surfactant concentration influenced monolayer thickness or dispersion stability, cit-GNRs were treated with 5 kDa mPEG-thiol in variable amounts. Stable dispersions were observed at loadings down to 15 μM (Figure 4a); the d_h mode peak did not change with mPEG concentration, ruling out the spontaneous formation of brush monolayers with extended chains.[45] Cit-GNRs treated with mPEG-thiol at or below 1.5 μM exhibited signs of aggregation several hours after treatment, based on the multimodal peak distribution in the NTA plots (Figure 4b). Again, the

dx.doi.org/10.1021/la502955h | Langmuir 2014, 30, 13737−13743

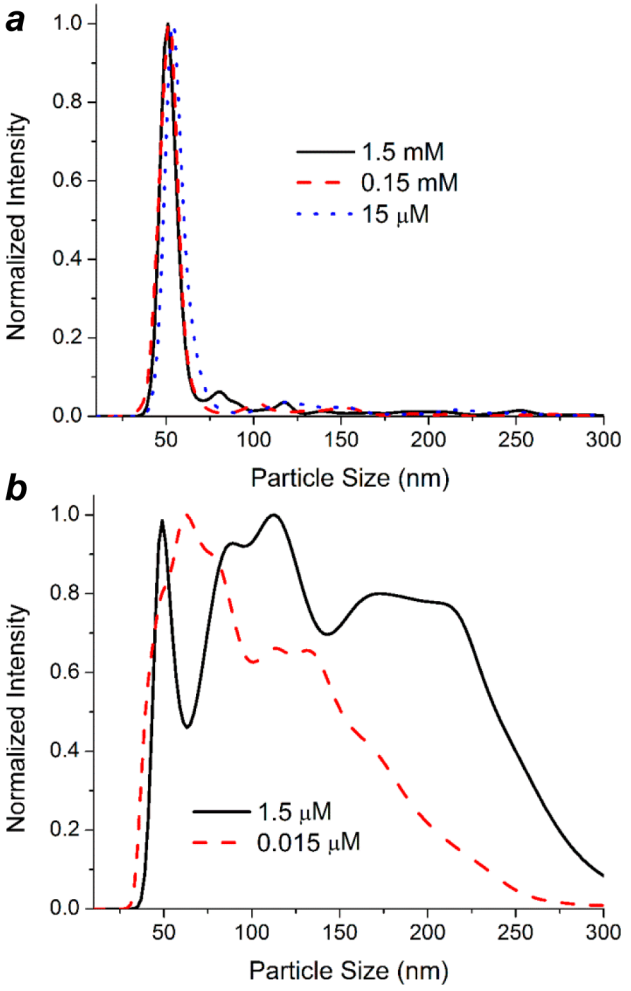

Figure 4. (a) Dispersion stability of GNRs at different exposure levels of 5 kDa mPEG-thiol. Intensities are normalized for a comparison between mode peaks as a function of preparation conditions. All mPEG-GNR samples were diluted 20−30-fold prior to NTA. (b) mPEG-thiol concentrations below 15 μM (0.075 mg/mL) were insufficient to produce fully dispersed GNRs, based on NTA.

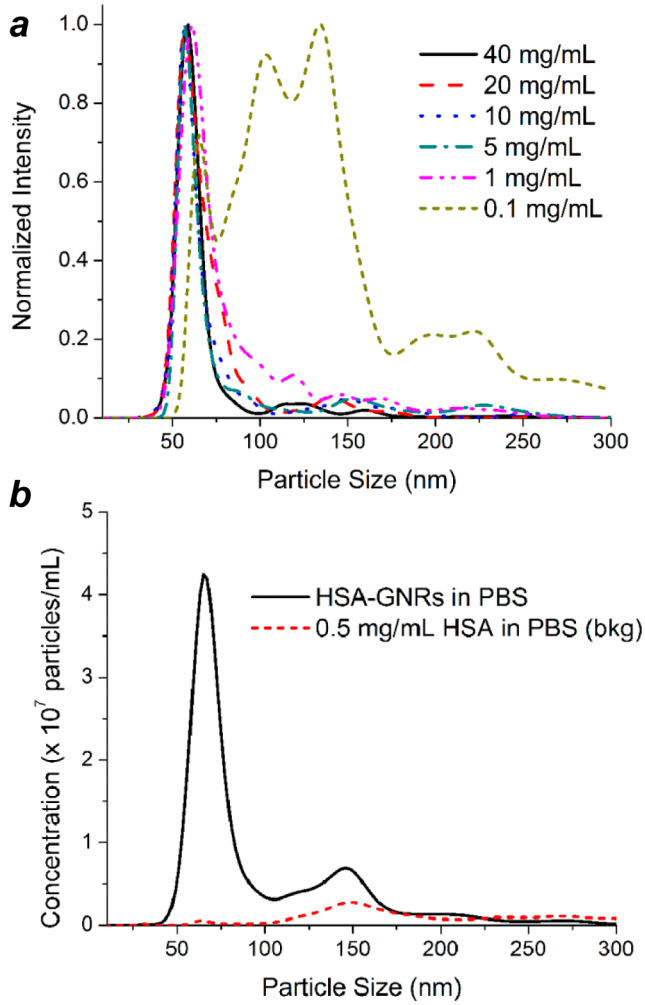

Figure 5. (a) GNRs exposed to different concentrations of HSA formed stable dispersions in water (d_h = 59−60 nm), down to 1 mg/mL. HSA-GNR samples (OD 1.9−2.0) were diluted 150-fold prior to NTA; intensities were normalized for a comparison between mode peaks. (b) GNRs dispersed in PBS ($I \sim 160$ mM) with 10 mg/mL HSA (d_h = 65 nm). HSA-GNRs (initial OD 0.4) were diluted 20-fold with PBS prior to NTA. A background run containing 0.5 mg HSA/mL in PBS is shown for comparison, to address the formation of protein aggregates.

absorbance spectra of these GNR dispersions were nearly indistinguishable from fully dispersed mPEG-GNRs (Figure S4, Supporting Information).

Concentration-dependent NTA studies using cit-GNRs and HSA in deionized water produced similar results, with an onset in GNR aggregation at 1 mg/mL HSA (Figure 5a). The mode peak of the coated GNRs did not shift with increasing amounts of HSA, in contrast to a recent NTA study of protein adsorption on spherical Au nanoparticles, which indicated concentration-dependent increases in HD size.[9] The low sensitivity to HSA concentration supports the notion that protein adsorption takes place preferentially at the GNR tips, in line with earlier studies on anisotropic functionalization.[24,27]

Similar results were observed for cit-GNRs treated with HSA in PBS, with the addition of a secondary peak centered at d_h = 150 nm (Figure 5b). This particle population can be attributed to the independent assembly of HSA nanoparticles at or near physiological ionic strength ($I \sim 160$ mM), as observed in the control study of 0.5 mg HSA/mL in the absence of cit-GNRs. It is worth mentioning that the HD size of HSA-coated GNRs did not increase further in dense protein solutions (up to 40 mg HSA/mL in PBS), indicating that HSA does not automatically form a protein multilayer (corona) around these particles. However, corona formation can be observed when cit-GNRs are exposed to serum proteins under other conditions, a study in progress that will be discussed elsewhere.

CONCLUSIONS

NTA is a valid method for measuring the hydrodynamic size of GNRs with low aspect ratios. The mode d_h value of citrate-stabilized GNRs matches closely with the mean length measured by TEM, indicating that translational diffusion is effectively isotropic under our imaging conditions. The NTA resolution of this study is approximately 5 nm, which is sufficient to measure differences in coating thickness based on HD size. In this respect, citrate-stabilized GNRs are dependable substrates for surface functionalization and ligand exchange, enabling a systematic analysis of GNR coatings as a function of surfactant structure and concentration.

dx.doi.org/10.1021/la502955h | *Langmuir* 2014, 30, 13737−13743

■ ASSOCIATED CONTENT

Supporting Information

Data for TEM size analysis, surfactant or ligand exchange using PSS- and cit-GNRs, and a sample videotrack of cit-GNRs with Brownian motion. This material is available free of charge via the Internet at http://pubs.acs.org.

■ AUTHOR INFORMATION

Corresponding Author

*Tel (765) 494-5257; e-mail alexwei@purdue.edu (A.W.).

Notes

The authors declare no competing financial interest.

■ ACKNOWLEDGMENTS

The authors gratefully acknowledge support from the National Cancer Institute (RC1 CA-147096), the Purdue University Center for Cancer Research (P30 CA023168), and the Birck Nanotechnology Center for DLS support. We also thank Anh Nguyen for TEM analysis, Gregory Knipp for providing HSA, and Ray Eby, Sonja Capracotta, Alan Rawle (Nanosight/Malvern), John Walker (Univ. Nottingham), and Stephan Link (Rice Univ.) for discussions on single-particle tracking analysis.

■ REFERENCES

(1) Bell, N. C.; Minelli, C.; Tompkins, J.; Stevens, M. M.; Shard, A. G. Emerging Techniques for Submicrometer Particle Sizing Applied to Stöber Silica. *Langmuir* **2012**, *28*, 10860−10872.

(2) Filipe, V.; Hawe, A.; Jiskoot, W. Critical Evaluation of Nanoparticle Tracking Analysis (NTA) by NanoSight for the Measurement of Nanoparticles and Protein Aggregates. *Pharm. Res.* **2010**, *27*, 796−810.

(3) Berne, B. J.; Pecora, R. *Dynamic Light Scattering: With Applications to Chemistry, Biology, and Physics*; Dover Publications: Mineola, 2000.

(4) Wei, A.; Mehtala, J. G.; Patri, A. K. Challenges and Opportunities in the Advancement of Nanomedicines. *J. Controlled Release* **2012**, *164*, 236−246.

(5) Kozak, D.; Anderson, W.; Vogel, R.; Chen, S.; Antaw, F.; Trau, M. Simultaneous Size and ζ-Potential Measurements of Individual Nanoparticles in Dispersion Using Size-Tunable Pore Sensors. *ACS Nano* **2012**, *6*, 6990−6997.

(6) Carr, B.; Wright, M. *Nanoparticle Tracking Analysis: A Review of Applications and Usage 2010 - 2012*; Nanosight Ltd.: Salisbury, UK, 2013.

(7) Mahl, D.; Diendorf, J.; Meyer-Zaika, W.; Epple, M. Possibilities and Limitations of Different Analytical Methods for the Size Determination of a Bimodal Dispersion of Metallic Nanoparticles. *Colloids Surf., A* **2011**, *377*, 386−392.

(8) Walker, J. G. Improved Nano-Particle Tracking Analysis. *Meas. Sci. Technol.* **2012**, *23*, 065605.

(9) James, A. E.; Driskell, J. D. Monitoring Gold Nanoparticle Conjugation and Analysis of Biomolecular Binding with Nanoparticle Tracking Analysis (NTA) and Dynamic Light Scattering (DLS). *Analyst* **2013**, *138*, 1212−1218.

(10) Arancon, R. A. D.; Lin, S. H. T.; Chen, G.; Lin, C. S. K.; Lai, J.; Xu, G.; Luque, R. Nanoparticle Tracking Analysis of Gold Nanomaterials Stabilized by Various Capping Agents. *RSC Adv.* **2014**, *4*, 17114−17119.

(11) Han, Y.; Alsayed, A. M.; Nobili, M.; Zhang, J.; Lubensky, T. C.; Yodh, A. G. Brownian Motion of an Ellipsoid. *Science* **2006**, *314*, 626−630.

(12) Han, Y.; Alsayed, A.; Nobili, M.; Yodh, A. G. Quasi-Two-Dimensional Diffusion of Single Ellipsoids: Aspect Ratio and Confinement Effects. *Phys. Rev. E* **2009**, *80*, 011403.

(13) Evans, D. F.; Wennerström, H. *The Colloidal Domain: Where Physics, Chemistry, Biology, and Technology Meet*, 2nd ed.; Wiley-VCH: New York, 1999.

(14) Pool, R.; Bolhuis, P. G. The Influence of Micelle Formation on the Stability of Colloid Surfactant Mixtures. *Phys. Chem. Chem. Phys.* **2010**, *12*, 14789−14797.

(15) Pollet, B.; Newton, J. E.; Preece, J. A.; Curnick, O. J. The Use of Ionic and Non-Ionic Surfactants for the Control of Platinum Nanoparticle Aggregation in Proton Exchange Membrane Fuel Cells (PEMFCS). *ECS Trans.* **2011**, *41*, 2165−2173.

(16) Sau, T. K.; Murphy, C. J. Seeded High Yield Synthesis of Short Au Nanorods in Aqueous Solution. *Langmuir* **2004**, *20*, 6414−6420.

(17) Khanal, B. P.; Zubarev, E. R. Rings of Nanorods. *Angew. Chem., Int. Ed.* **2007**, *46*, 2195−2198.

(18) Leonov, A. P.; Zheng, J.; Clogston, J. D.; Stern, S. T.; Patri, A. K.; Wei, A. Detoxification of Gold Nanorods by Treatment with Polystyrenesulfonate. *ACS Nano* **2008**, *2*, 2481−2488.

(19) Huff, T. B.; Hansen, M. N.; Zhao, Y.; Cheng, J.-X.; Wei, A. Controlling the Cellular Uptake of Gold Nanorods. *Langmuir* **2007**, *23*, 1596−1599.

(20) Mehtala, J. G.; Zemlyanov, D.; Max, J. P.; Kadasala, N.; Zhao, S.; Wei, A. Citrate-Stabilized Gold Nanorods. *Langmuir* **2014**, DOI: 10.1021/la5029542.

(21) Indrasekara, A. S. D. S.; Wadams, R. C.; Fabris, L. Ligand Exchange on Gold Nanorods: Going Back to the Future. *Part. Part. Syst. Charact.* **2014**, *31*, 819−838.

(22) Weisbecker, C. S.; Merritt, M. V.; Whitesides, G. M. Molecular Self-Assembly of Aliphatic Thiols on Gold Colloids. *Langmuir* **1996**, *12*, 3763−3772.

(23) Jain, P. K.; Eustis, S.; El-Sayed, M. A. Plasmon Coupling in Nanorod Assemblies: Optical Absorption, Discrete Dipole Approximation Simulation, and Exciton-Coupling Model. *J. Phys. Chem. B* **2006**, *110*, 18243−18253.

(24) Caswell, K. K.; Wilson, J. N.; Bunz, U. H. F.; Murphy, C. J. Preferential End-to-End Assembly of Gold Nanorods by Biotin-Streptavidin Connectors. *J. Am. Chem. Soc.* **2003**, *125*, 13914−13915.

(25) Hu, X.; Cheng, W.; Wang, T.; Wang, E.; Dong, S. Well-Ordered End-to-End Linkage of Gold Nanorods. *Nanotechnology* **2005**, *16*, 2164.

(26) Sudeep, P. K.; Joseph, S. T. S.; Thomas, K. G. Selective Detection of Cysteine and Glutathione Using Gold Nanorods. *J. Am. Chem. Soc.* **2005**, *127*, 6516−6517.

(27) Nie, Z.; Fava, D.; Kumacheva, E.; Zou, S.; Walker, G. C.; Rubinstein, M. Self-Assembly of Metal-Polymer Analogues of Amphiphilic Triblock Copolymers. *Nat. Mater.* **2007**, *6*, 609−614.

(28) Orendorff, C. J.; Hankins, P. L.; Murphy, C. J. pH-Triggered Assembly of Gold Nanorods. *Langmuir* **2005**, *21*, 2022−2026.

(29) Tirado, M. M.; Martinez, C. L.; de la Torre, J. G. Comparison of Theories for Translational and Rotational Diffusion Coefficients of Rod-Like Macromolecules. Application to short DNA fragments. *J. Chem. Phys.* **1984**, *81*, 2047−2052.

(30) Tcherniak, A.; Dominguez-Medina, S.; Chang, W.-S.; Swanglap, P.; Slaughter, L. S.; Landes, C. F.; Link, S. One-Photon Plasmon Luminescence and Its Application to Correlation Spectroscopy as a Probe for Rotational and Translational Dynamics of Gold Nanorods. *J. Phys. Chem. C* **2011**, *115*, 15938−15949.

(31) Mukhija, D.; Solomon, M. J. Translational and Rotational Dynamics of Colloidal Rods by Direct Visualization with Confocal Microscopy. *J. Colloid Interface Sci.* **2007**, *314*, 98−106.

(32) Cheong, F. C.; Grier, D. G. Rotational and Translational Diffusion of Copper Oxide Nanorods Measured with Holographic Video Microscopy. *Opt. Express* **2010**, *18*, 6555−6562.

(33) Hayat, M. A. *Colloidal Gold: Principles, Methods, and Applications*; Academic Press: San Diego, 1989; Vol. *1*.

(34) Wei, Q.; Wei, A. Signal Generation with Gold Nanoparticles: Photophysical Properties for Sensor and Imaging Applications. In *Supramolecular Chemistry of Organic−Inorganic Hybrid Materials*; Rurack, K., Mañez, R. M., Eds.; Wiley and Sons: New York, 2010; pp 319−349.

(35) Takahashi, H.; Niidome, Y.; Niidome, T.; Kaneko, K.; Kawasaki, H.; Yamada, H. Modification of Gold Nanorods Using Phosphatidylcholine to Reduce Cytotoxicity. *Langmuir* **2006**, *22*, 2−5.
(36) Yu, C.; Varghese, L.; Irudayaraj, J. Surface Modification of Cetyltrimethylammonium Bromide-Capped Gold Nanorods to Make Molecular Probes. *Langmuir* **2007**, *79*, 572−579.
(37) Wijaya, A.; Hamad-Schifferli, K. Ligand Customization and DNA Functionalization of Gold Nanorods Via Round-Trip Phase Transfer Ligand Exchange. *Langmuir* **2008**, *24*, 9966−9969.
(38) Rahme, K.; Chen, L.; Hobbs, R. G.; Morris, M. A.; O'Driscoll, C.; Holmes, J. D. Pegylated Gold Nanoparticles: Polymer Quantification as a Function of PEG Lengths and Nanoparticle Dimensions. *RSC Adv.* **2013**, *3*, 6085−6094.
(39) Basheva, E. S.; Kralchevsky, P. A.; Danov, K. D.; Ananthapadmanabhan, K. P.; Lips, A. The Colloid Structural Forces As a Tool for Particle Characterization and Control of Dispersion Stability. *Phys. Chem. Chem. Phys.* **2007**, *9*, 5183−5198.
(40) He, X. M.; Carter, D. C. Atomic Structure and Chemistry of Human Serum Albumin. *Nature* **1992**, *358*, 209−215.
(41) Goy-López, S.; Juárez, J.; Alatorre-Meda, M.; Casals, E.; Puntes, V. F.; Taboada, P.; Mosquera, V. Physicochemical Characteristics of Protein-NP Bioconjugates: The Role of Particle Curvature and Solution Conditions on Human Serum Albumin Conformation and Fibrillogenesis Inhibition. *Langmuir* **2012**, *28*, 9113−9126.
(42) Röcker, C.; Pötzl, M.; Zhang, F.; Parak, W. J.; Nienhaus, G. U. A Quantitative Fluorescence Study of Protein Monolayer Formation on Colloidal Nanoparticles. *Nat. Nanotechnol.* **2009**, *4*, 577−80.
(43) Elbakry, A.; Zaky, A.; Liebl, R.; Rachel, R.; Goepferich, A.; Breunig, M. Layer-by-Layer Assembled Gold Nanoparticles for siRNA Delivery. *Nano Lett.* **2009**, *9*, 2059−2064.
(44) Murthy, A. K.; Stover, R. J.; Hardin, W. G.; Schramm, R.; Nie, G. D.; Gourisankar, S.; Truskett, T. M.; Sokolov, K. V.; Johnston, K. P. Charged Gold Nanoparticles with Essentially Zero Serum Protein Adsorption in Undiluted Fetal Bovine Serum. *J. Am. Chem. Soc.* **2013**, *135*, 7799−7802.
(45) De Gennes, P. G. Polymers at an Interface; a Simplified View. *Adv. Colloid Interface Sci.* **1987**, *27*, 189−207.